Modelling of turbulent energy flux in canonical shock-turbulence interaction

Russell Quadros and Krishnendu Sinha

Indian Institute of Technology Bombay, Mumbai, India 400076

Abstract

High-speed turbulent flows often encounter high heat loads due to the presence of shock waves. The turbulent energy flux correlation in the mean energy conservation equation is a key unclosed term that determines the heat transfer rate. In this work, we employ existing turbulence models to predict the turbulent energy flux in canonical shock-turbulence interaction. The shortcomings of these models are highlighted, and a new heat-flux limiter model is proposed with the aid of linear theory results. We also write the transport equation for the turbulent energy flux across a shock wave and use it to develop a physics-based model for the same. It is found to predict the peak energy flux at the shock wave and its variation in the acoustic-adjustment region behind the shock. Numerical error incurred while solving the model equations at a shock wave are analyzed and a numerically robust model is obtained by eliminating the nonconservative source terms. The model predictions are compared with available direct numerical simulation data and a good match is obtained for a range of Mach numbers.

Keywords: High-speed flows, Heat transfer, Linear interaction analysis, RANS modelling

1. Introduction

High-speed flows in aerospace applications have shock waves interacting with boundary layers in different parts of the vehicle surface and in engine components. Such shock/boundary-layer interactions (SBLI) are often marked by high localized surface pressure and heat transfer rates [1, 2, 3]. Predicting the heating loads is especially important in supersonic and hypersonic applications with turbulent boundary layers. Majority of the existing turbulence models for heat flux prediction yield acceptable results in boundary-layer flows [4], but their predictive capability is severely limited in shock-dominated flows [5].

An important unclosed term in the mean energy conservation equation, which governs the heat transfer rate, is the turbulent energy flux vector $\widetilde{u_j''e''}$. Here, u_j'' represents the velocity fluctuation in the j^{th} direction, e'' represents the internal energy fluctuation and tilde represents Favre averaging. Conventionally, this term is modelled as a product of turbulent conductivity and the gradient of mean temperature. Turbulent conductivity is related to the eddy viscosity μ_T via a turbulent Prandtl number

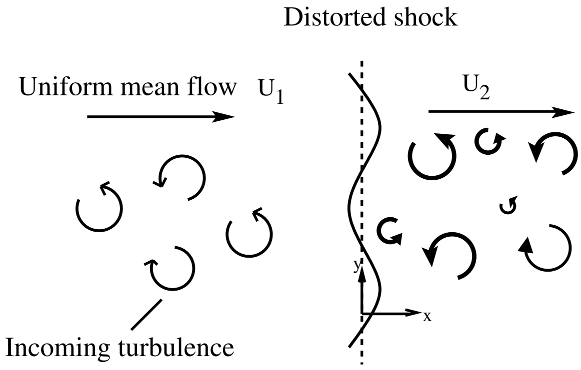

Figure 1: Schematic showing a shock wave distorted upon interaction with turbulent fluctuations.

Pr_T. A constant value of $Pr_T = 0.89$ gives satisfactory results in flat plate boundary layers and is often used in SBLI configurations. This modelling approach however significantly overpredicts the actual wall heat transfer rate in SBLI [5].

An alternate model based on variable Pr_T approach is proposed by Xiao et al. [6]. It solves additional differential equations for enthalpy variance and its dissipation rate, and employs these two quantities in the formulation of turbulent heat flux vector. In shock-dominated flows, this approach leads to improved wall heat flux predictions, yet it overpredicts experimental data. Sommer et al. [7] also develop a variable turbulent Prandtl number (Pr_T) model for high-speed compressible turbulent boundary layers with adiabatic and isothermal wall conditions. Other efforts in this direction are by Goldberg et al. [8], Aouissi et al. [9] and Abe and Suga [10]. Another notable work is by Bowersox [11], which proposes an algebraic model for the turbulent energy flux in supersonic flows, but is limited to zero-pressure-gradient boundary layers without shock waves.

In a recent work, Quadros et al. [12] present a detailed study of the turbulent energy flux at a shock wave. They investigate the physical processes that govern the generation of the energy flux correlation in a canonical shock-turbulence interaction (STI). This model problem consists of homogeneous isotropic turbulence, which is purely vortical in nature, being carried by a one-dimensional uniform mean flow passing through a nominally normal shock wave. The turbulence is amplified by the shock, and the shock in turn gets distorted. Schematic of this problem is shown in figure 1. This is possibly the simplest configuration that isolates the effect of shock on turbulence without other effects, such as boundary-layer gradient, flow separation and streamline curvature. In spite of its geometrical simplicity, STI displays a range of physical effects, such as, turbulence anisotropy, generation of acoustic waves, baroclinic torques, and unsteady shock oscillations.

The work presented in Quadros et al. [12] relies primarily on linear interaction analysis (LIA), a theoretical approach to analyse canonical STI. The analysis involves solving the fundamental interaction of a single two-dimensional plane wave with a shock, which generates downstream disturbances that can be characterised in terms of Kovasznay modes of vorticity, entropy and acoustic [13]. Integration over a specified upstream turbulence spectrum yields three-dimensional turbulence statistics downstream of the shock. The LIA results obtained for the energy flux are compared with direct numerical simulation (DNS) data available from Larsson et al. [14]. The results show a rapid non-monotonic variation behind the shock wave, and a peak positive value of the correlation in the near-field acoustic adjustment region.

Quadros et al. [12] also compute the budget of the energy flux transport equation using the DNS data. It is found that the rapid post-shock variation of the turbulent energy flux is governed by inviscid-linear mechanisms, and there is negligible effect of the viscous and non-linear terms to the overall budget. The linear inviscid theory is able to predict the dominant mechanisms and thus can be effectively used for developing advanced physics-based models for turbulent energy flux generated at shock waves. This is similar to the LIA-based modelling of the turbulent kinetic energy amplification at shock waves [15, 16], and the resulting shock-unsteadiness model has shown significant improvements in SBLI predictions [17, 18, 19].

In another recent work, Quadros et al. [20] study the correlation coefficient R_{uT} between streamwise velocity and temperature fluctuations in canonical shock-turbulence interaction. R_{uT} is a key link in modelling of turbulent energy flux. As per the strong Reynolds analogy, the velocity and temperature fluctuations are anti-correlated, i.e. $R_{uT} = -1$. This assumption corresponds to a value of turbulent Prandtl number $Pr_T = 1$, which is close to the value used in practice. In the presence of shock waves, Morkovin's hypothesis is not valid [21], and R_{uT} can vary significantly. Quadros et al. [20] present the variation of R_{uT} with Mach number, turbulent Mach number and Reynolds number, as predicted using linear inviscid theory and compare to the data from DNS. Different types of incoming disturbances – purely vortical, vortical/entropy and vortical/acoustic – are also considered.

Quadros et al. [20] decompose the velocity-temperature correlation coefficient in terms of the three Kovasznay modes of vorticity, entropy and acoustic. The contributions from the individual Kovasznay modes are quantified, and compared with available DNS data. At low Mach numbers, it is found that the peak post-shock R_{uT} is determined by the acoustic mode, which is correctly predicted by the linear theory. At high Mach numbers, the post-shock R_{uT} is determined primarily by the vorticity and entropy modes, which are strongly affected by nonlinear and viscous effects, and thus less well predicted by linear theory.

In this paper, we investigate different modelling strategies to predict the turbulent energy flux generated by shock-homogeneous turbulence interaction. It is based on the physical understanding of how the turbulent energy flux evolves across a shock wave, at varying Mach and Reynolds numbers, as per our recent works summarized in section 2. We consider existing turbulence models, including conventional gradient diffusion and realizable models (section 3). We also develop new models based on linear inviscid theory (section 4) and study their numerical behaviour at shock waves (section 5).

2. Turbulent energy flux in shock-turbulence interaction

Quadros et al. [12] studied the generation of turbulent energy flux in canonical STI problem using LIA, which models the upstream turbulence as a collection of planar waves. Each of these waves is considered to independently interact with the shock. The governing equations downstream of the shock are linearized Euler equations and the jump in fluctuations across the shock is given by linearised inviscid Rankine-Hugoniot conditions.

A set of linear algebraic equations are obtained by substituting the planar waveforms

M_1	M_t	Re_λ	$R_{kk}/(2U_1^2)$	$\kappa_\circ L_\epsilon$	$k_0 \times 10^2$	$\epsilon_0 \times 10^3$	$k_1 \times 10^2$	$\epsilon_1 \times 10^3$	$\kappa_\circ \delta_s$
1.28	0.22	38	7.3×10^{-3}	3.9	2.98	1.17	2.42	0.92	1.75
1.50	0.22	38	5.3×10^{-3}	3.9	2.88	1.12	2.42	0.92	1.30
1.87	0.22	39	6.9×10^{-3}	3.8	2.78	1.08	2.42	0.92	1.18
2.50	0.22	40	4.0×10^{-3}	4.3	2.69	1.03	2.42	0.92	0.86
3.50	0.22	40	2.1×10^{-3}	4.3	2.61	1.00	2.42	0.92	0.45
4.70	0.23	42	1.2×10^{-3}	4.3	2.56	0.97	2.42	0.92	0.43
6.00	0.23	42	0.7×10^{-3}	4.4	2.53	0.96	2.42	0.92	0.36

Table 1: DNS cases from Larsson et al. [14] with mean Mach number, turbulent Mach number and Reynolds number listed at a location just upstream of the shock. The peak wavenumber $\kappa_\circ$ is used to normalize the dissipation length scale L_ϵ and the DNS mean shock thickness δ_s. Also given are the non-dimensional values of turbulence kinetic energy k and dissipation rate ϵ at the inlet station (subscript 0) and just before the shock (subscript 1).

into the governing equations. Solving these equations yields the disturbance field downstream of the shock for a given upstream vortical wave. The downstream turbulent field for a full three-dimensional upstream turbulence is obtained by integrating the two-dimensional planar wave results over a specified energy spectrum. Details of this analysis can be found in Mahesh et al. [22].

DNS of canonical STI was carried out by Larsson et al. [14] for vortical turbulence passing through a normal shock. Table 1 lists the DNS cases used in the current study. The Mach numbers range from low supersonic to hypersonic values. Turbulent Mach number M_t and Reynolds number based on Taylor scale Re_λ for each of the cases are also listed. Here, turbulent Mach number is defined as $M_t = \sqrt{R_{kk}}/\widetilde{a}$, where R_{kk} represents twice the turbulence kinetic energy, and $\widetilde{a}$ represents the Favre-averaged speed of sound. Re_λ is given by $\overline{\rho}\sqrt{R_{kk}/3}\lambda/\overline{\mu}$, where λ is the Taylor scale and $\overline{\mu}$ is the average dynamic viscosity.

Figure 2(a) compares the streamwise variation of the turbulent energy flux obtained from DNS and LIA for $M_1 = 1.50$ (reproduced from Quadros et al. [12]). Note that conventional Reynolds averaging/fluctuation is used instead of its Favre counterpart, as negligible difference is observed upon comparison using the DNS data set. The shock is centered at $x = 0$ with the unsteady shock movement region highlighted using two vertical lines. We normalize the streamwise distance with dissipation length scale L_ϵ, calculated just upstream of the shock as

$$L_\epsilon = (R_{kk}/2)^{3/2}/\epsilon, \tag{1}$$

where ϵ is the dissipation rate of turbulence kinetic energy, and the values of $\kappa_\circ L_\epsilon$ for DNS are listed in table 1. Since viscous dissipation is absent in the linear theory, the equivalent dissipation length scale is obtained by using the most energetic

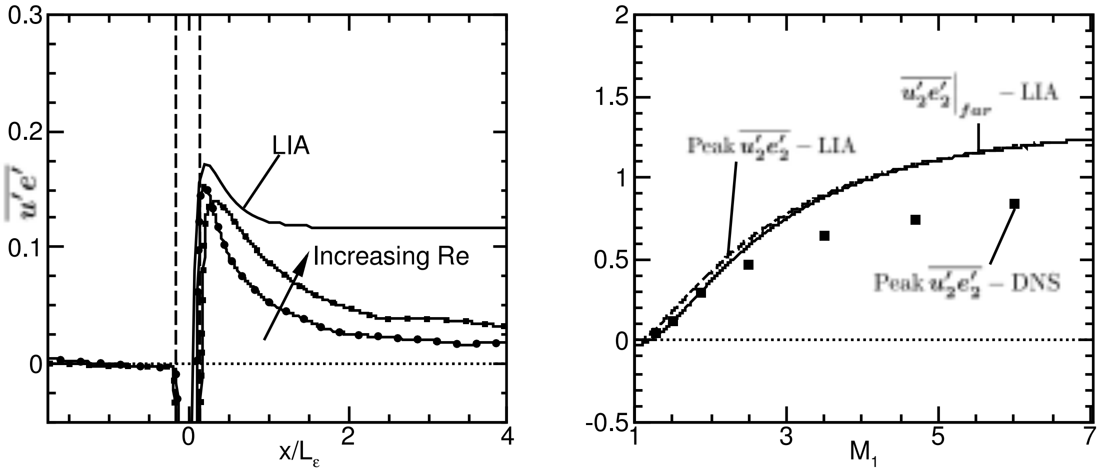

(a)

(b)

Figure 2: Turbulent energy flux generated in shock-turbulence interaction. (a) Streamwise variation of turbulent energy flux for $M_1 = 1.5$ from LIA (lines) and DNS (line-symbols) with $M_t = 0.15$. Effect of Reynolds number is also shown with $Re_\lambda = 40$ (circle) and $Re_\lambda = 75$ (square). $x = 0$ represents the center of the mean shock thickness, and the vertical lines near $x = 0$ represent the mean shock thickness region. (b) Variation of peak $\overline{u_2'e_2'}$ with upstream Mach number. The DNS data corresponds to $M_t = 0.22$ and $Re_\lambda = 40$. The velocity fluctuations are normalized by the upstream mean velocity and the energy fluctuations are normalized by the product of the downstream mean temperature and the specific gas constant R. The correlation is further normalized by upstream turbulence kinetic energy.

wavenumber ($\kappa_\circ$) in the expression $\kappa_\circ L_\epsilon \approx 3 - 4$ obtained from the DNS study [14].

Upstream of the shock, DNS shows a negligible value of turbulent energy flux, and in the region of the unsteady shock wave, it predicts large negative values of the correlation. Just downstream of the shock, both LIA and DNS predict a peak positive energy flux. Further downstream, DNS shows a steep decrease in the energy flux values to negligible levels, whereas LIA predicts a constant far-field value. With increasing Reynolds number, the DNS data tends to approach the LIA prediction, which is representative of $Re \to \infty$ limit. The peak turbulent energy flux obtained from DNS at two Reynolds numbers are comparable in magnitude, and their location are close to each other, when the streamwise coordinate is normalized by the dissipation length scale. This is not the case when Kolmogorov scale is used to non-dimensionalize the distance from the shock wave.

The peak value of turbulent energy flux $\overline{u_2'e_2'}$ (subscript 2 indicates the shock-downstream values) as predicted by both DNS and LIA for varying Mach numbers is shown in figure 2(b), reproduced from Quadros et al. [12]. Also shown is the far-field asymptotic value of LIA, and at high Mach numbers, it is almost equal to the LIA peak energy flux. The peak energy flux as per theory matches well with DNS for low Mach numbers upto $M_1 < 2$, with the theory overpredicting the values at higher shock strengths. The LIA prediction reaches an asymptotic value of 1.32 at high Mach numbers, while DNS shows a limiting value less than 1. The DNS data is found to approach the LIA predictions with

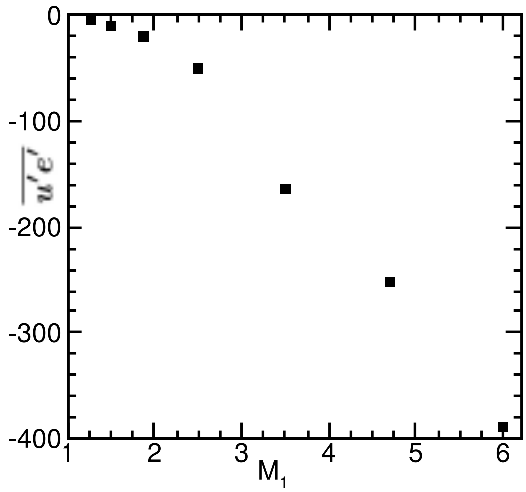

Figure 3: Peak turbulent energy flux for varying upstream Mach numbers as predicted by conventional model with the shock-thickness taken from the DNS data. The results correspond to turbulent Mach number $M_t = 0.22$ just before the shock. Normalisation as described in figure 2.

decreasing turbulent Mach number (lower non-linear effects); see Quadros et al. [12] for further details. Overall, a good qualitative match is observed between LIA and DNS indicating that the key physical mechanisms governing the energy flux transport are captured by the theory.

3. Existing models for turbulent energy flux

3.1. Conventional Modelling

The turbulent energy flux is conventionally modelled using the gradient diffusion hypothesis as

$$\overline{u'e'} = -\frac{\kappa_T}{\overline{\rho}} \frac{\partial \widetilde{T}}{\partial x}, \tag{2}$$

where $\overline{\rho}$ and $\widetilde{T}$ are mean density and temperature. Thermal conductivity κ_T is given by $\kappa_T = \mu_T c_v / Pr_T$, where c_v is the specific heat at constant volume and Pr_T represents the turbulent Prandtl number having a constant value of 0.89. Eddy viscosity is given by $\mu_T = c_\mu^\circ \overline{\rho} k^2/\epsilon$, where $c_\mu^\circ = 0.09$, k is turbulence kinetic energy (TKE). In order to compute for the turbulent energy flux in the given model problem, the mean flow variables are prescribed as hyperbolic tangent profiles across the shock, with the shock thickness obtained from the DNS data. The values of k and ϵ used in the expression for eddy viscosity are obtained by solving the corresponding differential equations [15] using a fourth order Runge-Kutta (RK4) method, with the inlet boundary condition specified from the DNS data. The resulting values for k and ϵ match well with DNS as reported in earlier works [15, 16].

The value of the energy flux obtained using (2) is zero in the region upstream and downstream of the shock due to uniform mean flow temperature on either side of the normal shock. However, the energy flux assumes a peak negative value in the region of the shock, and the peak values obtained for a range of upstream Mach number are shown in figure 3. In the limit of $M_1 \to 1$, the value of the energy flux predicted by the model reduces to zero, and with increasing Mach number, the magnitude of the negative peak rises to a value that is almost two orders of magnitude higher than the post-shock DNS predictions. Also, in a CFD framework, this formulation yields a grid-dependent value of the energy flux in the region of the shock From (2), $\overline{u'e'} \sim \Delta\widetilde{T}/\delta_s \sim \Delta\widetilde{T}/\Delta x$, where $\Delta\widetilde{T}$ is the jump in the mean temperature across the shock, δ_s is the mean shock thickness and Δx is the local grid resolution. Increasing the grid point density (decreasing Δx) therefore increases the magnitude of the negative peak.

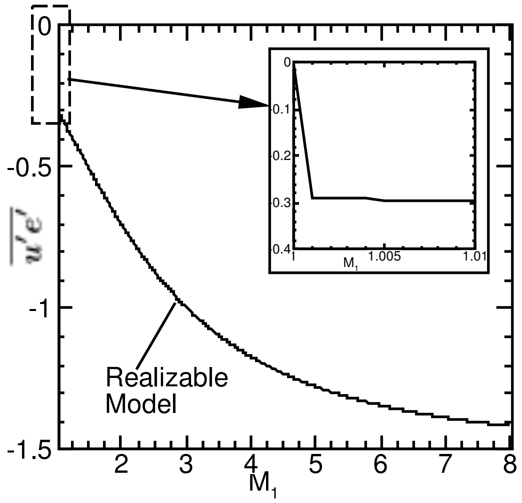

Figure 4: Variation of peak turbulent energy flux with upstream Mach number as predicted by realizable model with shock thickness taken from the DNS data. The peak value is independent of the shock thickness, which is indicative of a grid-independent solution in a CFD simulation. Normalisation as described in figure 2.

3.2. Realizable Model

In canonical shock-turbulence interaction, the Reynolds stress as predicted by the conventional model is given by [15]

$$\overline{\rho u'u'} = -\frac{4}{3}\mu_T \frac{\partial \widetilde{u}}{\partial x} + \frac{2}{3}\overline{\rho}k. \qquad (3)$$

This modelling approach leads to unphysically high values of TKE in the region of shock due to its proportionality with the mean velocity gradient. The realizability correction limits the value of eddy viscosity in the region of shock through the form $c_\mu = \min(c_\mu^o, \sqrt{c_\mu^o}/s)$ [23], where $s = S/(\epsilon/k)$, $S = \sqrt{(2S_{ij}S_{ji} - (2/3)S_{kk}^2)}$ and $S_{ij} = (\partial\widetilde{u}_i/\partial x_j + \partial\widetilde{u}_j/\partial x_i)/2$. In the region of high gradients such as shock $c_\mu = (\sqrt{c_\mu^o}\epsilon)/(Sk)$ and therefore

$$\mu_T = \frac{\sqrt{3c_\mu^o}}{2}\frac{\overline{\rho}k}{\left|\frac{\partial \widetilde{u}}{\partial x}\right|}. \qquad (4)$$

Thus the expression for energy flux given by (2) reduces to

$$\overline{u'e'} = -\frac{\sqrt{3c_\mu^0}}{2}\frac{kc_v}{Pr_T\left|\frac{\partial\widetilde{u}}{\partial x}\right|}\frac{\partial\widetilde{T}}{\partial x}, \qquad (5)$$

in the shock region.

The value of TKE as well as the mean variables required for the above formulation are obtained as described in the previous section. Similar to the conventional model, the realizable model yields a zero value of energy flux outside the region of shock. However, inside the shock region, a peak negative value is obtained as per (5). This peak energy flux value for varying Mach number is plotted in figure 4. For almost all Mach numbers, the realizable model predicts a negative energy flux in the shock region, but the magnitude is restricted due to the realizability constraint, and is of the same order as the post-shock DNS value. Contrary to the eddy viscosity formulation, the realizability limiter yields a peak value of energy flux which is independent of the shock thickness assumed. This is because $\overline{u'e'} \sim (\Delta\widetilde{T}/\delta_s)/(\Delta\widetilde{u}/\delta_s) \sim \Delta\widetilde{T}/\Delta\widetilde{u}$, assuming k to be finite, as predicted in Sinha et al. [15]. Thus, in a real CFD simulation, the peak value in the shock region will be insensitive to grid refinement. In the limit of $M_1 \to 1$, the realizable model switches to the conventional model formulation and predicts a value of zero energy flux as shown in the inset figure. In the limit of $M_1 \to \infty$, the model saturates to a negative limiting value, a trend similar to the DNS data, but opposite in sign.

4. New physics-based models

4.1. Algebraic heat flux limiter model

We use linear interaction analysis results to propose an algebraic model for turbulent energy flux at the shock as

$$\overline{u'e'} = \beta \frac{k c_v}{\left|\frac{\partial \widetilde{u}}{\partial x}\right|} \frac{\partial \widetilde{T}}{\partial x}. \qquad (6)$$

This form is similar to the realizability constraint shown in (4), with β as an unknown modelling parameter. From the mean energy conservation equation across the shock, we can write

$$\widetilde{u} \left| \frac{\partial \widetilde{u}}{\partial x} \right| = c_p \frac{\partial \widetilde{T}}{\partial x}, \qquad (7)$$

where c_p is the specific heat at constant pressure. Substituting the above equation in (6) yields

$$\overline{u'e'} = \frac{\beta k \widetilde{u}}{\gamma}, \qquad (8)$$

where the turbulent energy correlation is seen to be proportional to turbulent kinetic energy. This is physically consistent with the linear theory results that show all correlations generated across the shock to be directly proportional to the upstream TKE.

Further, the normalised expression for energy flux can be written as

$$\overline{u'e'}|_{Norm.} = \frac{\overline{u'e'}}{R \widetilde{u}_1 \widetilde{T}_2 \frac{k_1}{\widetilde{u}_1^2}}, \qquad (9)$$

where R is the specific gas constant. The energy flux is normalized in this manner throughout this work, and the subscript $Norm.$ is dropped for convenience. Using (8) with the upstream values of k and U, along with (9), simplifies the above expression to

$$\overline{u'e'} = \beta \frac{M_1^2}{T_r}, \qquad (10)$$

where T_r is the mean temperature ratio across the shock. In the high Mach number regime, this ratio is proportional to M_1^2,

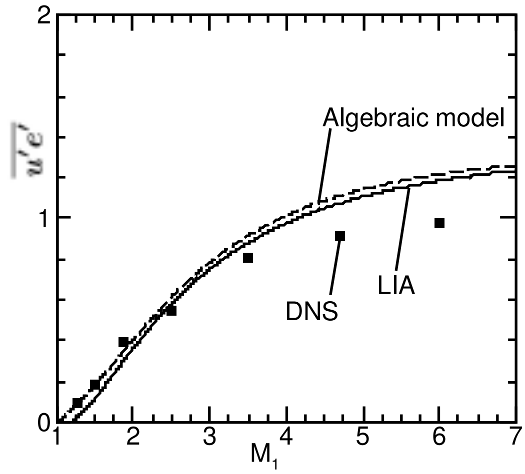

Figure 5: Variation of $\overline{u'e'}$ with upstream Mach number as per new algebraic formulation. Also seen are the DNS values of energy flux extrapolated to the shock center and the far-field LIA results. Normalisation as described in figure 2.

and the above expression obtains a limiting value

$$\overline{u'e'} = \beta \frac{(\gamma+1)^2}{2\gamma(\gamma-1)}. \qquad (11)$$

A similar trend is observed in DNS and LIA, where the peak turbulent energy flux saturates at high Mach numbers. In order to find the value of the modelling parameter β, we equate (11) to the LIA far-field limiting value of 1.4. This gives a value of $\beta = 0.27$ for $\gamma = 1.4$. However, in the limit of $M_1 \to 1$, the energy flux attains a value equal to 0.27, which is physically incorrect. On the contrary, the energy flux predicted by the conventional model in the $M_1 \to 1$ limit is zero (as $\overline{u'e'}$ is proportional to the mean temperature gradient), which is consistent with the DNS and LIA predictions. We therefore propose a low Mach number correction of the form

$$\beta' = (1 - e^{1-M_1})\beta, \qquad (12)$$

which yields $\beta' = 0$ as $M_1 \to 1$ and $\beta' \to \beta$ as $M_1 \to \infty$.

Figure 5 shows the model predictions of the peak turbulent energy flux for a range of upstream Mach numbers. Also shown in the figure are the downstream DNS values of energy flux extrapolated to the shock center and the far-field LIA values. The model matches well with DNS for $M_1 < 2$, and for higher Mach numbers, it is close to LIA and overpredicts the DNS values.

4.2. Differential-equation based model

In this section, we propose a differential-equation based model to predict the turbulent energy flux in STI. The model development is based on the linear theory approximations, and it builds on the fact that the peak turbulent energy flux behind the shock is reproduced well by LIA. The model is developed in two parts. The first part attempts to predict the peak turbulent energy flux generated behind the shock, and the second part reproduces the decay of the energy flux further downstream. The model is developed in conjunction with the model equations for TKE and its dissipation rate proposed by Sinha et al. [15]. The closure coefficients are obtained from the LIA results, as in the earlier works [15, 24, 16], and the model predictions are compared with available DNS data [14]. The equation for the conservation of total enthalpy across the shock wave can be written in terms of the shock-normal velocity component u_n as

$$\frac{\partial h_e}{\partial x} + u_n \frac{\partial u_n}{\partial x} = 0, \qquad (13)$$

where h_e is the enthalpy. For an unsteady distorted shock wave of the form presented in figure 1, $u_n \simeq \overline{u} + u' - \xi_t$, which assumes small deviation of the shock wave from its mean location. Here, ξ represents the shock displacement from its mean position, and ξ_t represents the local streamwise velocity

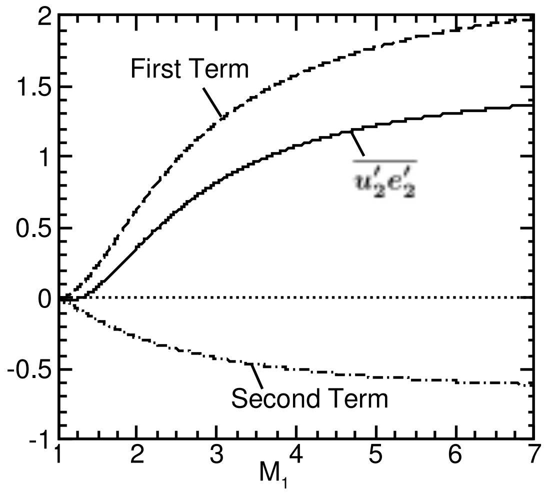

Figure 6: Variation of $\overline{u_2'e_2'}$ with upstream Mach number as predicted by (16) along with the individual contributions of the source terms. Normalisation as described in figure 2.

of the shock wave; see Sinha [16] for further details. Linearising the above equation in terms of fluctuations in enthalpy h' and streamwise velocity u', we get

$$\frac{\partial h'}{\partial x} + \overline{u}\frac{\partial u'}{\partial x} + u'\frac{\partial \overline{u}}{\partial x} - \xi_t \frac{\partial \overline{u}}{\partial x} = 0. \qquad (14)$$

Taking a moment with u' and Reynolds averaging yields a differential equation for the energy flux correlation.

$$\gamma \frac{\partial}{\partial x}\overline{u'e'} = -\overline{u'^2}\frac{\partial \overline{u}}{\partial x} + \overline{u'\xi_t}\frac{\partial \overline{u}}{\partial x} - \overline{u}\frac{\partial}{\partial x}\frac{\overline{u'^2}}{2} + \overline{h'\frac{\partial u'}{\partial x}}, \qquad (15)$$

where the enthalpy fluctuations are replaced by the internal energy fluctuations via $h' = \gamma e'$. The first term on the RHS represents the generation of turbulent energy flux due to mean compression in the shock wave, and the second term brings in the shock-unsteadiness effect. The change in the streamwise Reynolds stress across the shock contributes to the turbulent energy flux via the third term on the RHS. The last term is a correlation of the enthalpy fluctuations with the change in the streamwise velocity fluctuations across the shock.

The first two source terms are analogous to the production and the shock-unsteadiness damping terms in the TKE equation presented in Sinha et al. [15]. We follow their modelling approach to write $\overline{u'\xi_t} = b_1\overline{u'^2}$, which is based on the assumption that the unsteady shock oscillations are caused by the incoming velocity fluctuations. The streamwise Reynolds stress is then closed in terms of the turbulence kinetic energy by considering its isotropic form i.e., $\overline{u'^2} = 2k/3$ [15]. The final model equation for the turbulent energy flux thus takes the form

$$\frac{\partial}{\partial x}\left(\overline{u'e'}\right) = -\frac{2(1-b_1)}{3\gamma}k\frac{\partial \overline{u}}{\partial x} - \frac{1}{3\gamma}\overline{u}\frac{\partial k}{\partial x}, \tag{16}$$

where $b_1 = 0.4 + 0.6\exp(2(1-M_1))$. The last term is dropped from the equation for want of an adequate closure approximation.

The value of turbulent energy flux is obtained by numerically integrating (16) over prescribed hyperbolic tangent shock profiles of the mean variables. Figure 6 shows the value of turbulent energy flux obtained across the shock for varying upstream Mach numbers. The correlation takes a value of zero as $M_1 \to 1$, which is physically consistent with negligible turbulent energy flux across very weak shocks. With increase in upstream Mach number, the energy flux gradually rises to saturate in the $M_1 \to \infty$ limit. The contribution of both the terms on the RHS of (16) are also shown in the figure. While the first model term in the above equation generates a positive turbulent energy flux across the shock wave, the second term has a negative contribution to the energy flux correlation. The magnitude of the first term is significantly higher than the second for all upstream Mach numbers, therefore yielding a positive value of the energy flux.

Now consider the differential equation governing the jump in TKE at the shock given by the shock-unsteadiness model [15]

$$\overline{\rho}\widetilde{u}\frac{\partial k}{\partial x} = -\frac{2}{3}\overline{\rho}k\frac{\partial \widetilde{u}}{\partial x}(1-b_1). \tag{17}$$

Also, from the mean energy conservation equation across the shock, we can write

$$\widetilde{u}\left|\frac{\partial \widetilde{u}}{\partial x}\right| = c_p\frac{\partial \widetilde{T}}{\partial x}. \tag{18}$$

Using the above two equations, (16) can be written as

$$\frac{\partial}{\partial x}\left(\overline{u'e'}\right) = c_{ue}\left(\frac{k}{\overline{\widetilde{u}}}\right)c_p\frac{\partial \widetilde{T}}{\partial x}, \tag{19}$$

where $c_{ue} = 4(1-b_1)/(9\gamma)$ and $\widetilde{u} \simeq \overline{u}$. This equation is compact with only one modelled term governing the value of energy flux across the shock. Moreover, similar to the conventional form discussed earlier, the energy flux is modelled in terms of the gradient in the mean temperature. Figure 7 compares the energy flux values as predicted by (19) for varying upstream Mach numbers with the far-field LIA results and the downstream DNS values of energy flux extrapolated to the shock center. The model prediction attains a value of zero as $M_1 \to 1$ and saturates to a positive limiting value at high Mach numbers similar to the DNS and LIA results. A good match is observed with the LIA results, and the model overpredicts in comparison with the DNS data for higher upstream Mach numbers. In order to model the decay in the turbulent energy flux behind the shock, we look at the mechanisms responsible for its post-shock evolution. Quadros et al. [12] study the

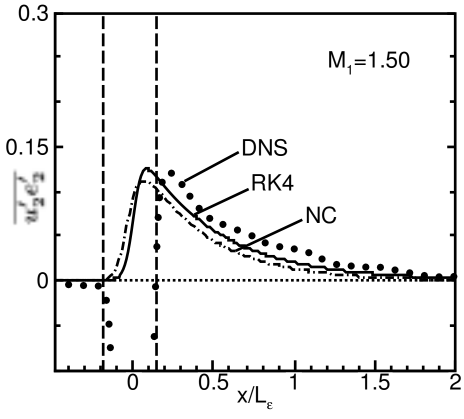

(a)

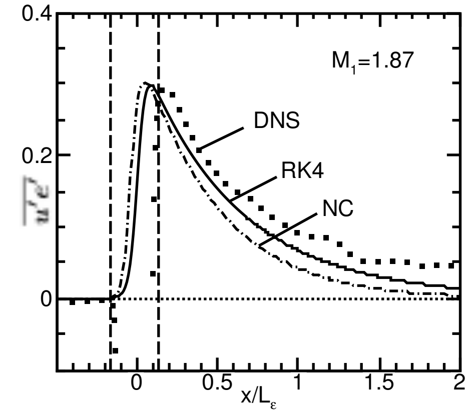

(b)

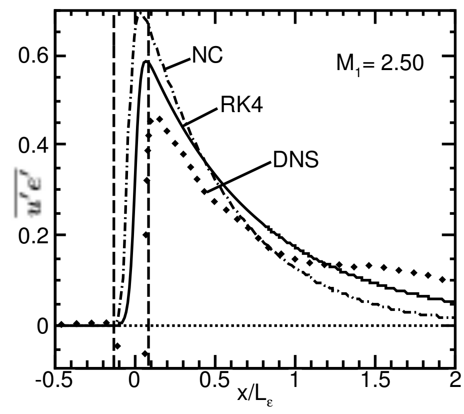

(c)

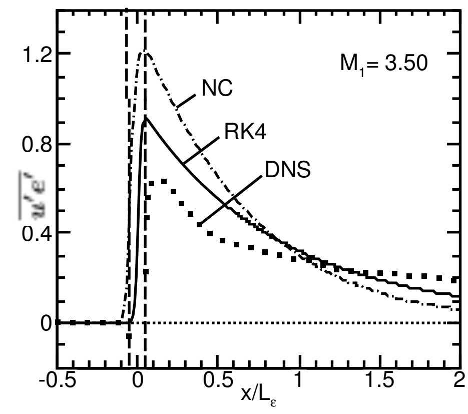

(d)

Figure 8: Streamwise variation of $\overline{u'e'}$ as computed using Runge-Kutta (RK4) method (line) and the Lax-Friedrich scheme (dash-dot) for the nonconservative (NC) form of transport equation, compared with the DNS data (symbols) for four upstream Mach numbers. The vertical lines near $x/L_\epsilon = 0$ represent the mean shock thickness. Normalisation as described in figure 2.

budget of $\overline{u'e'}$ transport equation in the linear inviscid framework, which yields

$$\overline{\rho}\,\widetilde{u}\frac{\partial}{\partial x}\overline{u'e'} = \underbrace{-\ \overline{e'\frac{\partial p'}{\partial x}}}_{\text{Press. energy}}\ \underbrace{-\ \overline{p}\,\overline{u'\frac{\partial u_j'}{\partial x_j}}}_{\text{pressure-dilatation}}, \tag{20}$$

i.e., the post-shock turbulent energy flux is determined by the pressure-energy and pressure-dilatation mechanisms. In the region behind the shock ($0 < x/L_\epsilon < 1$), these processes are dominated by the acoustic mode, for which the thermodynamic fluctuations can be assumed to be approximately isentropic. Therefore, the pressure-energy term can be written as [12]

$$-\overline{e'\frac{\partial p'}{\partial x}} = -\frac{1}{\gamma\overline{\rho}}\frac{\partial}{\partial x}\left(\frac{\overline{p'^2}}{2}\right),$$

which corresponds to the streamwise variation of pressure variance. The pressure-dilatation term in (20) is proportional to the mean post-shock pressure, and the

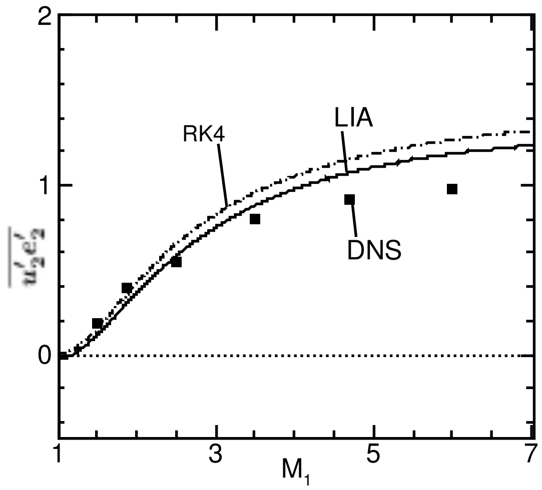

Figure 7: Variation of $\overline{u_2'e_2'}$ with upstream Mach number as predicted by (19) using the Runge-Kutta (RK4) integration method. Also shown are the corresponding DNS values extrapolated to shock center and far-field LIA results. Normalisation as described in figure 2.

$\overline{u'(\partial u_j'/\partial x_j)}$ correlation can be expanded as

$$\overline{u'\frac{\partial u_j'}{\partial x_j}} = \frac{\partial}{\partial x}\frac{\overline{u'^2}}{2} + \overline{u'\frac{\partial v'}{\partial y}} + \overline{u'\frac{\partial w'}{\partial x}}.$$

The first term on the RHS represents the buildup of streamwise Reynolds stress as a result of the acoustic decay, and can be argued to be positive in the acoustic-adjustment region behind the shock.

Data from DNS and LIA [20] show that the pressure variance $\overline{p'^2}$ decays exponentially behind the shock, and the same can be expected for $\overline{u'e'}$. This decay can be modelled by adding a term proportional to $-\overline{u'e'}/L$ to the RHS of the $\overline{u'e'}$ transport equation. Here, the characteristic decay length scale L is taken as the dissipation length scale L_ϵ, which is representative of the large acoustic scales in the turbulence field. The full model equation for the energy flux thus takes the following form

$$\frac{\partial}{\partial x}\left(\overline{u'e'}\right) = c_{ue}\left(\frac{k}{\widetilde{\widetilde{u}}}\right) c_p \frac{\partial \widetilde{T}}{\partial x} - c_2\frac{\overline{u'e'}}{L_\epsilon}, \quad (21)$$

where $c_2 = 0.3 + 3\exp(1 - M_1)$ is a modelling parameter based on the DNS data.

Figure 8 shows the streamwise variation of the turbulent energy flux for four upstream Mach numbers, obtained by numerically integrating (21) using the fourth-order Runge-Kutta (RK4) method. The shock is specified as a hyperbolic tangent profile of the mean flow variables; it is centered at $x = 0$, with the thickness obtained from the DNS data (shown using two vertical lines). The turbulent energy flux in the incoming flow is set to zero for the purely vortical turbulence upstream of the shock wave.

The model predicts a peak positive value of the correlation across the shock, and we observe a good match between the model prediction and the DNS data for $M_1 = 1.5$ and 1.87. For the Mach 2.5 case, the model overpredicts the peak $\overline{u'e'}$ observed in DNS, but matches the post-shock decay rate up to $x = L_\epsilon$. At the highest Mach number interaction considered here ($M_1 = 3.5$), the model overpredicts the peak value as well as the decay rate behind the shock for $x < L_\epsilon$. Further downstream, we see a systematic under-prediction for all Mach numbers, and it is most prominent for the Mach 2.5 case. This can be attributed to the fact that the majority of the pressure fluctuations decay within $x \simeq L_\epsilon$, and further decay of $\overline{u'e'}$ is possibly governed by viscous dissipation. The current model, without any viscous effects, is unable to reproduce $\overline{u'e'}$ outside the acoustic decay region behind the shock.

5. Numerical simulation

The model predictions presented above are obtained by numerically integrating the model equations for specified mean flow profiles across a shock wave. The integration step size is kept small so that the results are devoid of numerical error. On the other hand, in computational fluid dynamic simulations presented below, the mean flow variables at a shock wave are computed as part of the solution, and are prone to numerical error. In this section, we assess the effect of the numerical error on the turbulent energy flux prediction and device ways to eliminate them.

5.1. Numerical methodology

We solve the one-dimensional Reynolds-averaged Navier-Stokes equations for the mean flow, and the shock-unsteadiness k-ϵ model from Sinha et al. [15] is used for turbulence closure. The diffusive fluxes are neglected because their contribution is expected to be small in the current shock-turbulence interaction [25]. The governing equations are cast in a non-dimensional form, where the upstream mean speed of sound and mean density are taken as the characteristic quantities. The most energetic wave number $\kappa_0 = 4$ in the incoming turbulence field is taken as the characteristic length scale.

The mean conservation equations along with the $k - \epsilon$ and $\overline{u'e'}$ model equations are solved using the finite volume approach, where the equations are written in a vector form.

$$\frac{\partial}{\partial t}\underbrace{\begin{Bmatrix} \overline{\rho} \\ \overline{\rho}\,\widetilde{u} \\ \widetilde{E} \\ \overline{\rho}\,k \\ \overline{\rho}\,\overline{\epsilon} \\ \overline{\rho}\,\overline{u'e'} \end{Bmatrix}}_{[\mathrm{U}]} + \frac{\partial}{\partial x}\underbrace{\begin{Bmatrix} \overline{\rho}\,\widetilde{u} \\ \overline{\rho}\,\widetilde{u}^2 + \overline{p} \\ \widetilde{u}(\widetilde{E} + \overline{p}) \\ \overline{\rho}\,\widetilde{u}\,k \\ \overline{\rho}\,\widetilde{u}\,\epsilon \\ \overline{\rho}\,\widetilde{u}\,\overline{u'e'} \end{Bmatrix}}_{[\mathrm{F}]} = \underbrace{\begin{Bmatrix} 0 \\ 0 \\ 0 \\ -(2/3)\overline{\rho}k(\partial\widetilde{u}/\partial x)(1 - b_1') - \overline{\rho}\epsilon \\ -(2/3)c_1\overline{\rho}\epsilon(\partial\widetilde{u}/\partial x) - c_{\epsilon 2}\overline{\rho}(\epsilon^2/k) \\ c_{ue}(k/\widetilde{u})c_p(\partial\widetilde{T}/\partial x) - c_2(\overline{u'e'}/L_\epsilon) \end{Bmatrix}}_{[\mathrm{S}]}. \tag{22}$$

Here, [U] is the vector of the conserved variables, [F] is the vector containing the inviscid fluxes and [S] is the vector containing the source terms, where tilde represents Favre averaging and $\widetilde{E}$ is the mean total energy.

The inviscid fluxes at cell faces are evaluated using the Lax-Friedrich scheme and the turbulent source terms are evaluated at the cell centers. The mean flow gradients in the production terms are discretized using a second-order accurate central difference scheme. Explicit time integration is achieved using the first order forward Euler method. The Lax-Friedrich method is more dissipative than the modified Steger Warming method used by Sinha and Balasridhar [25], but can produce identical results with larger number of grid points.

We simulate shock-turbulence interaction for varying shock-strength, i.e. Mach number ranging from low supersonic to hypersonic values (see table 1). The turbulent Mach number M_t just upstream of the shock wave is taken as 0.22. The normalized turbulence kinetic energy is thus given by $k_1 = M_t^2/2$, where subscript 1 represents shock-upstream values. The Reynolds number based on Taylor microscale $Re_\lambda = \lambda u'_{rms}/\nu = 40$ [26], where $u'_{rms} = \sqrt{2k/3}$. The Taylor microscale is given by $\lambda = \sqrt{10\nu k/\epsilon}$, where ν is the mean kinematic viscosity of the fluid. The turbulent dissipation rate ϵ can thus be computed as

$$\epsilon_1 = \frac{5}{\sqrt{3}}\left(\frac{M_t^3}{\kappa_0\lambda}\right)\frac{1}{Re_\lambda}, \tag{23}$$

where $\kappa_0\lambda = 0.84$.

The computational domain extends from $\kappa_\circ x = -7.6$ to 29.6, with the shock centered at $x = 0$. The homogeneous turbulence upstream of the shock follows decay relations

$$\widetilde{u}\frac{dk}{dx} = -\epsilon,$$
$$\widetilde{u}\frac{d\epsilon}{dx} = -c_{\epsilon 2}\frac{\epsilon^2}{k},$$

with solution given by

$$\begin{aligned} k_0 &= k_1\left[1 + \kappa_0 x_{sh}\frac{(c_{\epsilon 2}-1)}{M_1}\frac{\epsilon_0}{k_0}\right]^{\frac{1}{c_{\epsilon 2}-1}}, \\ \epsilon_0 &= \epsilon_1\left[1 + \kappa_0 x_{sh}\frac{(c_{\epsilon 2}-1)}{M_1}\frac{\epsilon_0}{k_0}\right]^{\frac{c_{\epsilon 2}}{c_{\epsilon 2}-1}}, \end{aligned} \tag{24}$$

where k_0 and ϵ_0 are the inlet values obtained from the shock upstream values (see table 1). The same values are used to initialize the turbulence variables in the simulation. Here, $c_{\epsilon 2} = 1.2$ and $\kappa_0 x_{sh} = 6.83$. The mean flow quantities are initialized to Rankine-Hugoniot jump conditions at the shock at $x = 0$. At the exit boundary, we specify zero gradient boundary condition for all the mean flow and turbulence variables.

5.2. Numerical results

The mean flow and the model equations are solved using 800 points equally spaced along the shock-normal direction. The jump in the turbulent energy flux for varying Mach numbers is presented in figure 9. For low Mach numbers upto $M_1 = 2$, there is a good match between the Lax-Friedrich and the RK4 solution reproduced from figure 7. However, at higher Mach numbers, the numerical scheme overpredicts the jump in the turbulent energy flux. The reason for this can be attributed to the error in the numerical solution computed at the shock. The earlier results obtained for a specified tangent hyperbolic shock profile is devoid of such numerical error. The numerical error is not found to decrease with successive grid refinement; see results obtained using 400, 800 and 1200 grid points in figure 9. A similar trend is observed with the $k - \epsilon$ solution at shock waves [25] and is discussed below. The streamwise variation of the turbulent energy flux obtained by solving (21) numerically is shown in figure 8. The results are compared with the RK4 method and the corresponding DNS data. For the low Mach number case of $M_1 = 1.50$, both the RK4 and the numerical solution match well and are comparable to the DNS data. With increasing Mach number, the numerical solution deviates from the RK4 result both in the jump across the shock and the downstream evolution. This deviation once again can be attributed to the nonconservative error in the source terms of the transport equation for k, ϵ and $\overline{u'e'}$.

Sinha and Balasridhar [25] studied the numerical issues involved while solving shock-turbulence interaction using the shock-unsteadiness k-ϵ equations. It was found that for shock capturing simulations, like those in this work, the nonconservative

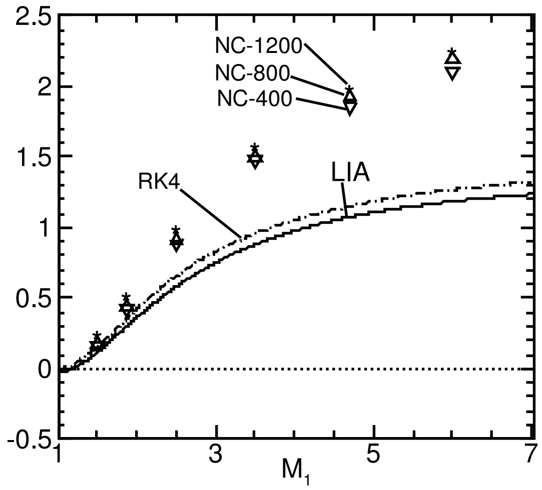

Figure 9: The post-shock turbulent energy flux as computed using the Lax-Friedrich scheme applied to the nonconservative (NC) form of the model equations, compared with the Runge-Kutta (RK4) method and linear theory (LIA) predictions. Solution computed on different grid sizes: 400 (gradient), 800 (triangle), 1200 (star). Normalisation as described in figure 2.

nature of the production terms can result in large numerical error at shock waves. The inviscid flux terms, on the other hand, are in conservative form. In a finite-volume approach, the fluxes are evaluated at cell interfaces. The corresponding truncation error involves higher-order derivatives of the flow variables, which take large values in the shock wave. It is shown that the error from adjacent cells cancel at the common interfaces when all the finite volume cells spanning the shock wave are taken together. The net error across the shock wave is therefore a function of the higher-order derivatives evaluated in a region of smooth flow solution, outside the shock wave. On successive grid refinement, the leading-error term vanishes and the solution tends towards the exact integral. Further details can be found in the appendix of Sinha and Balasridhar [25].

The source terms in both the k and ϵ equations involve flow derivatives that are evaluated using a symmetric second-order discretization Sinha and Balasridhar [25]. The corresponding truncation error involves third and higher-order derivatives of velocity, pressure and temperature. On integration over a finite volume cell, the corresponding error term thus involves integration of these higher order derivatives. The leading error term scales as $1/\delta^3$, where δ is the computed shock thickness, and hence the error takes large values in the region of a flow discontinuity. When all the finite volume cells spanning the shock wave are taken together, these error terms from the individual cells add up and appear as numerical volume sources. Unlike the conservative flux terms, the telescopic effect of error cancellation between adjacent cells is absent in the nonconservative source terms [25]. This leads to significant error that are comparable or larger than the physical production at the shock waves. Also, the numerical error does not decrease in magnitude with successive grid refinement as observed for smooth solutions.

To restrict the truncation errors at shock waves, Sinha and Balasridhar [25] proposes an alternative form of the shock-unsteadiness k-ϵ equations obtained by transforming the turbulence variables. Conserved quantities involving k and ϵ are formulated and transport equations for these new variables are derived. The new $k-\epsilon$ equations capture identical physics as the original shock-unsteadiness model, but are free of the nonconservative source terms, and therefore show dramatic improvement in numerical accuracy. Here, we follow a similar approach for the $\overline{u'e'}$ model equation given in (21) to derive the corresponding conservative form.

5.3. Conservative formulation

A conservative formulation of the governing equations for k and ϵ is derived by Sinha and Balasridhar [25], and is given as

$$\overline{\rho}\,\widetilde{u}\frac{\partial f}{\partial x} = -\rho\epsilon\rho^{-(2/3)c_o}, \quad (25)$$

$$\overline{\rho}\,\widetilde{u}\frac{\partial g}{\partial x} = \frac{-c_{\epsilon 2}\epsilon^2}{k}\rho^{1-(2/3)c_1}, \quad (26)$$

where $c_o = 1 - b_1'$ and $b_1' = 0.4(1 - exp(1 - M_1))$, and the transformed variables $f = k\rho^{-\frac{2}{3}c_o}$ and $g = \epsilon\rho^{-\frac{2}{3}c_1}$ are based on the closed form solution of the original equations. Solving the above two equations instead of their corresponding nonconservative forms significantly improved the prediction of TKE and its dissipation rate in canonical STI; see Sinha and Balasridhar [25] for details. A closed form solution for energy flux can be obtained by writing (19) as

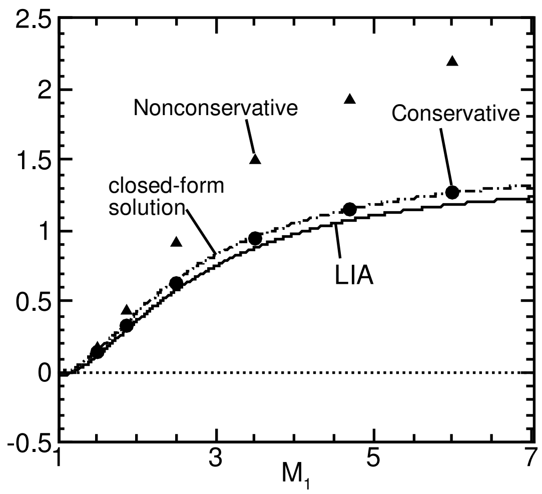

Figure 10: Comparison of the turbulent energy flux computed using the Lax-Friedrich scheme applied to the conservative and nonconservative forms of the model equations with the closed-form solution and the far-field LIA values. Normalisation as described in figure 2.

$$\frac{\partial}{\partial x}\left(\overline{u'e'}\right) = \frac{c_{ue}c_p}{\overline{\rho}\widetilde{u}}f\rho^{(2c_0/3+1)}\frac{\partial\widetilde{T}}{\partial x}, \quad (27)$$

where f is a conserved variable across the shock [25]. This equation reduces to

$$\frac{\partial}{\partial x}\left(\overline{u'e'}\right) = -c_{ue}f(\overline{\rho}\,\widetilde{u})^{2c_0/3}\widetilde{u}^{-2c_0/3}\frac{\partial\widetilde{u}}{\partial x}, \quad (28)$$

using the total energy conservation across a shock wave. Integrating between the shock-upstream (subscript 1) and shock-downstream (subscript 2) locations yields

$$\overline{u_2'e_2'} = A_1\left[\widetilde{u}_2^{1-2c_0/3} - \widetilde{u}_1^{1-2c_0/3}\right], \quad (29)$$

where $A_1 = -c_{ue}f(\overline{\rho}\widetilde{u})^{2c_0/3}/(1-2c_0/3)$ is a conserved quantity across the shock. The value of the energy flux predicted by this closed form solution is plotted for varying upstream Mach numbers in figure 10. A good match is observed with the solution obtained by solving the corresponding differential equation (19) using RK4 method as shown in figure 9.

The closed form solution is used to define a new variable

$$h = \overline{u'e'} - A_1\widetilde{u}^{1-2c_0/3}, \quad (30)$$

and write the model equation for $\overline{u'e'}$ as

$$\frac{\partial h}{\partial x} = -c_2\frac{\overline{u'e'}}{L_\epsilon}, \quad (31)$$

which captures the same physics as the original equation (21), but is numerically more robust at shock waves than the former. This is because the nonconservative source terms involving the mean temperature derivative is eliminated from the transport equation. Numerical implementation of the conservative model equations follow the same method as described in (22), with k, ϵ and $\overline{u'e'}$ replaced by f, g and h, respectively. The source term vector $[S]$ is appropriately modified as per the right-hand sides of (25), (26) and (31). The initial and boundary conditions are recast in terms of the transformed variables, and the turbulence variables k, ϵ and $\overline{u'e'}$ are obtained from the solution by invoking the reverse transformation.

Figure 10 shows the peak turbulent energy flux for varying upstream Mach number obtained by numerically solving the conservative form of the model equations. The results match exactly with the closed form solution and are a significant improvement over the nonconservative results. Figure 11 shows the streamwise evolution of the turbulent energy flux computed on different numerical grids. The data corresponds to the higher Mach number cases, where the nonconservative error is most prominent. The results show a systematic grid convergence, with the difference in the peak $\overline{u'e'}$ values diminishing with successive grid refinement. The model predictions also compare well with the DNS data up to $x \simeq L_\epsilon$ for the Mach 2.5 interaction and upto $x \simeq 0.7L_\epsilon$ for the high Mach number case. Turbulent energy flux predicted for the Mach 1.5 and 1.87 flows are almost identical to those in figure 8, and they are also comparable to the post-shock DNS data.

Figure 10 shows the peak turbulent energy flux for varying upstream Mach number obtained by numerically solving the conservative form of the model equations. The results match exactly with the closed form solution and are a significant improvement over the nonconservative results. Figure 11 shows the streamwise evolution of the turbulent energy flux computed on different numerical grids. The data corresponds to the higher Mach number cases, where the nonconservative error is most prominent. The results show a systematic grid convergence, with the difference in the peak $\overline{u'e'}$ values diminishing with successive grid refinement. The model predictions also compare well with the DNS data up to $x \simeq L_\epsilon$ for the Mach 2.5 interaction and upto $x \simeq 0.7L_\epsilon$ for the high Mach number case. Turbulent energy flux predicted for the Mach 1.5 and 1.87 flows are almost identical to those in figure 8, and they are also comparable to the post-shock DNS data.

6. Conclusion

In this paper, we look at various modelling strategies to predict the turbulent energy flux generated in canonical shock-turbulence interaction. Application of conventional $k - \epsilon$ models based on the gradient diffusion hypothesis yields large negative value of energy flux in the shock region, which rises drastically with increasing Mach number and grid refinement. These values are much higher in magnitude than the post-shock DNS predictions, which yield a low positive energy flux. Realizable model also predicts negative values of the energy flux in the shock region, but the peak value is limited by the realizability constraint. A new model is proposed using results from linear interaction analysis, which has been shown to capture the key physics of turbulent energy flux generated at a shock wave. The model is based on a heat-flux limiter formulation similar in form to the realizability constraint and is able to predict the peak turbulent energy flux over a range of Mach numbers. We also develop a transport equation model for the turbulent energy flux, based on the linear and inviscid interaction of turbulent fluctuations with a shock wave. The model parameters are taken from the well-established shock-unsteadiness $k - \epsilon$ model,and a numerically robust form is proposed by elimi-

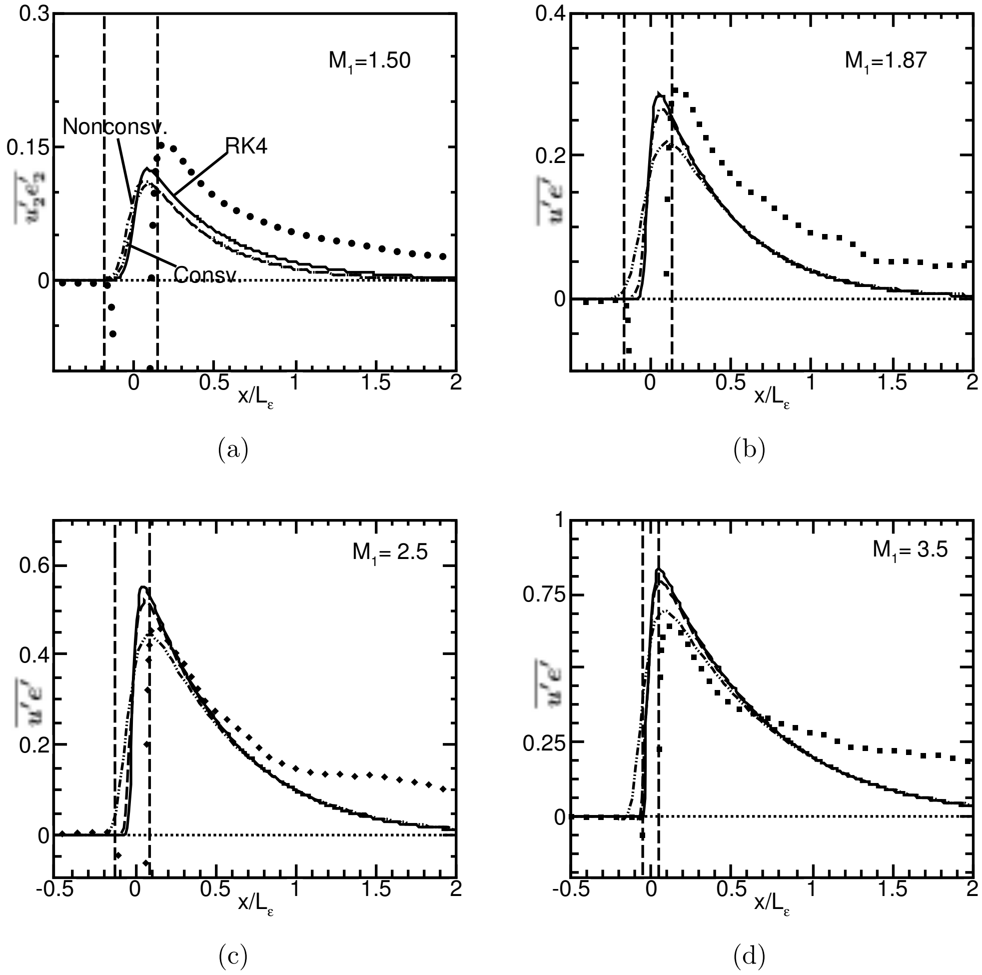

Figure 11: Streamwise variation of $\overline{u'e'}$ as computed using the conservative form of the model equations are compared with the DNS data (symbols) for two upstream Mach numbers. The vertical lines near $x/L_\epsilon = 0$ represent the mean shock thickness, and the Lax-Friedrich scheme is employed on three different grids: 400 (dash dot dot), 800 (dash) and 1200 (solid). Normalisation as described in figure 2.

nating the nonconservative source terms in the equation. The new physics-based model is found to predict DNS values of the peak energy flux correlation and the acoustic decay downstream of the shock wave.

References

[1] D. V. Gaitonde, Progress in shock wave/boundary layer interactions, Progress in Aerospace Sciences 72 (2015) 80 – 99.

[2] V. Pasquariello, M. Grilli, S. Hickel, N. A. Adams, Large-eddy simulation of passive shock-wave/boundary-layer interaction control, International Journal of Heat and Fluid Flow 49 (2014) 116 – 127.

[3] J. Quaatz, M. Giglmaier, S. Hickel, N. Adams, Large-eddy simulation of a pseudo-shock system in a Laval nozzle, International Journal of Heat and Fluid Flow 49 (2014) 108 – 115.

[4] J. L. Brown, Turbulence Model Validation for Hypersonic Flows, 8^{th} AIAA/ASME Joint Thermophysics and Heat Transfer Conference, St. Louis, MO .

[5] C. J. Roy, F. G. Blottner, Review and assessment of turbulence models for hypersonic flows, Progress in Aerospace Sciences 42 (7)

(2001) 469–530.

[6] X. Xiao, H. A. Hassan, J. R. Edwards, R. L. G. Jr., Role of turbulent Prandtl numbers on heat flux at hypersonic Mach numbers, AIAA Journal 45 (4) (2007) 806–813.

[7] T. P. Sommer, R. M. C. So, H. S. Zhang, Near-Wall Variable-Prandtl-Number Turbulence Model for Compressible Flows, AIAA Journal 31 (1) (1993) 27–35.

[8] U. C. Goldberg, S. Palaniswamy, P. Batten, V. Gupta, Variable turbulent Schmidt and Prandtl number modeling, Engineering application of computational fluid mechanics 4 (2010) 511.

[9] M. Aouissi, A. Bounif, K. Bensayah, Scalar turbulence model investigation with variable turbulent Prandtl number in heated jets and diffusion flames, Heat Mass Transfer 44 (2008) 1065.

[10] K. Abe, K. Suga, Towards the development of a Reynolds-averaged algebraic turbulent scalar-flux model, International Journal of Heat and Fluid Flow 22 (2001) 19–29.

[11] R. D. W. Bowersox, Extension of equilibrium turbulent heat flux models to high-speed shear flows, J. Fluid Mech. 633 (2009) 61–70.

[12] R. Quadros, K. Sinha, J. Larsson, Turbulent energy flux generated by shock/homogeneous-turbulence interaction, accepted in J. Fluid Mech. .

[13] L. S. G. Kovasznay, Turbulence in supersonic flow, J. Aeronaut. Sci. 20 (10) (1953) 657–674.

[14] J. Larsson, I. Bermejo-Moreno, S. K. Lele, Reynolds- and Mach number effects in canonical shock-turbulence interaction, J. Fluid Mech. 717 (2013) 293–321.

[15] K. Sinha, K. Mahesh, G. V. Candler, Modeling shock-unsteadiness in shock-turbulence interaction, Phys. Fluids 15 (2003) 2290–2297.

[16] K. Sinha, Evolution of enstrophy in shock/homogeneous turbulence interaction, J. Fluid Mech. 707 (2012) 74–110.

[17] K. Sinha, K. Mahesh, G. V. Candler, Modeling the effect of shock unsteadiness in shock-wave / turbulent boundary-layer interactions, AIAA Journal 43 (3) (2005) 586–594.

[18] A. A. Pasha, K. Sinha, Shock-unsteadiness model applied to oblique shock-wave/turbulent boundary-layer interaction, Int. J. Comput. Fluid Dyn. 22 (8) (2008) 569–582.

[19] A. A. Pasha, K. Sinha, Shock-unsteadiness model applied to hypersonic shock-wave/turbulent boundary-layer interactions, Journal of Propulsion and Power 28 (1) (2012) 46–60.

[20] R. Quadros, K. Sinha, J. Larsson, Kovasznay mode decomposition of velocity-temperature correlation in canonical shock-turbulence interaction, accepted in Flow, Turbulence and Combustion .

[21] K. Mahesh, S. K. Lele, P. Moin, The influence of entropy fluctuations on the interaction of turbulence with a shock wave, J. Fluid Mech. 334 (1997) 353–379.

[22] K. Mahesh, S. K. Lele, P. Moin, The interaction of a shock wave with a turbulent shear flow, Tech. Rep. 69, Thermosciences division, Department of Mechanical Engineering, Stanford University, Stanford, CA., 1996.

[23] F. Thivet, D. D. Knight, A. A. Zheltovodov, A. I. Maksimov, Importance of limiting the turbulent stresses to predict 3D shock-wave/boundary-layer interactions, 23rd International Symposium on Shock Waves, Fort Worth, TX .

[24] V. K. Veera, K. Sinha, Modelling the effect of upstream temperature fluctuations on shock/homogeneous turbulence interaction, Phys. Fluids 21 (2009) 025101.

[25] K. Sinha, S. J. Balasridhar, Conservative formulation of the $k - \epsilon$ turbulence model for shock-turbulence interaction, AIAA Journal 51 (8) (2013) 1872–1882.

[26] H. Tennekes, J. L. Lumley, in: A First Course in Turbulence, The MIT press, 1972.